Rare Metal Materials and Engineering
Volume.50, Issue.4, April 2021
Available online at **www.rmme.ac.cn**

Science Press

Cite this article as: Wang Yuxiang, Zhong Shengwen, Wen Xiaoqiang, et al. Synthesis and Luminescent Properties of $Y_2O_2SO_4$:Eu^{3+} Sub-micron Rods[J]. Rare Metal Materials and Engineering, 2021, 50(04):1204-1209.

Synthesis and Luminescent Properties of $Y_2O_2SO_4$:Eu^{3+} Sub-micron Rods

Wang Yuxiang[1,2], Zhong Shengwen[1], Wen Xiaoqiang[2], Zhang Qian[1]

[1] College of Materials Metallurgy and Chemistry, Jiangxi University of Science and Technology, Ganzhou 341000, China; [2] Ganzhou Nonferrous Metallurgy Research Institute, Ganzhou 341000, China

Abstract: One-dimensional $Y_2O_2SO_4$:Eu^{3+} sub-micron rods were synthesized by a facial molten-salt method with Na_2SO_4 and K_2SO_4 as the eutectic melt. The crystallography, morphology and luminescence properties of as-synthesized products were characterized by X-ray powder diffraction (XRD), scanning electronic microscope (SEM) and photoluminescence (PL) spectra. The influence of the sintering temperature and Eu^{3+} doping concentration on the crystallography, morphology, and luminescence properties of the samples was investigated. The results show that pure $Y_2O_2SO_4$:Eu^{3+} can be prepared by calcining the raw material mixture at 1100 °C for 2 h in air. The monoclinic $Y_2O_2SO_4$:Eu^{3+} (10mol%) sub-micron rods have a length more than 10 μm and a width of 500~800 nm. The photoluminescence spectra of the $Y_2O_2SO_4$:Eu^{3+} sub-micro rods confirm the strongest red emission peak at 616 nm upon the excitation of 270 nm ultraviolet light, which corresponds to the $^5D_0 \rightarrow {}^7F_2$ transition of Eu^{3+}. Moreover, the quenching concentration mechanism of $Y_2O_2SO_4$:Eu^{3+} samples with Eu^{3+} above 10mol% was also discussed.

Key words: molten-salt method; $Y_2O_2SO_4$:Eu^{3+} sub-micron rods; europium doping

In the past decade, Rare earth oxysulfates ($Ln_2O_2SO_4$, Ln represents rare earth) have attracted great attention for its important physical properties[1,2]. In particular, lanthanide oxysulfate is a good matrix due to its low phono-energy, high quantum yields, adequate thermal, and environmental stability. Introducing different rare-earth ions into appropriate inorganic hosts as activators is a useful strategy to obtain the required phosphors[3]. Rare-ions doped $Ln_2O_2SO_4$:Re^{3+} as a high-performance luminescent material that can be excited by ultraviolet light or X-ray has aroused a lot of attention owing to its advantages such as good chemical and structural stability, high luminous efficiency, and simple preparation process[4-7]. Currently, Eu^{3+} has become one of the most common and widespread activators in modern lighting and display fields based on their intra-configurational 4f transitions. The emission wavelength of Eu^{3+} doped $Y_2O_2SO_4$ is about 616 nm, which can be used in the field of red light-emitting display.

Different methods have been reported for the synthesis of luminescent materials with good performance. $Y_2O_2SO_4$:Re^{3+} luminescent materials can be prepared via template method[8], conventional solid-state reaction[9], thermal decomposition method[10], electrospinning[11], hydrothermal way[12], co-precipitation process[13]. However, the materials prepared by these methods usually have some weaknesses, which reduce their luminescent performance.

In the past few years, one-dimensional rare-earth luminescent materials have various potential applications from photochemistry and photophysics to data storage and optoelectronic devices[14-16]. However, there are few reports on the synthesis of one-dimensional $Y_2O_2SO_4$:Eu^{3+} red luminous materials. In this work, we employed the molten salt synthesis method[17-20], which has a low synthesis temperature and short reaction time, to prepare one-dimensional $Y_2O_2SO_4$:Eu^{3+} sub-micron rods with good luminescent properties. The purity and phase composition of the samples were also well controlled. The liquid environment provided by the molten salt is favorable for the growth of crystals, and the molten salt prevents the agglomeration of particles[21-24]. The as-prepared $Y_2O_2SO_4$:Eu^{3+} sub-micron rods sintered at 1100 °C have a width of 500~800 nm and a length more than 10 μm, and the strongest red emission peak at 616 nm upon 270 nm ultraviolet light excitation, which is caused by the $^5D_0 \rightarrow {}^7F_2$ transition of Eu^{3+}. The

Received date: April 25, 2020
Foundation item: National Natural Science Foundation of China (51874151)
Corresponding author: Zhong shengwen, Ph. D., Professor, College of Materials Metallurgy and Chemistry, Jiangxi University of Science and Technology, Ganzhou 341000, P. R. China, E-mail: zhongsw-jxust@outlook.com

simplicity of this synthetic approach makes it promising for the preparation of other RE activated phosphors.

1 Experiment

Y_2O_3, Eu_2O_3, $(NH_4)_2SO_4$, Na_2SO_4, and K_2SO_4 were used as the starting materials. The stoichiometric Y_2O_3, Eu_2O_3, and $(NH_4)_2SO_4$ powders were mixed in an agate mortar for 1 h with a certain amount of Na_2SO_4 and K_2SO_4. The mixture was sintered at different temperatures (950 °C to 1150 °C) for 2 h in a corundum crucible. The as-synthesized phosphor powders were crushed and washed with deionized water for several times until the molten salt was completely removed. Finally, the obtained powders were dried at 100 °C for 5 h.

The phase composition of the samples was measured with the D/max-rA type rotating target X-ray diffractometer from 10° to 60°. The phosphor particle morphologies were determined by Zeiss scanning electron microscope. The elemental distribution was determined with energy-dispersive X-ray spectroscopy (EDS). The excitation and emission spectra of the samples were obtained at room temperature by Hitachi F-7000 fluorescence spectrometer. The excitation light source was 150 W Xenon lamp with a scanning speed of 240 nm min^{-1} and a resolution of 1.0 nm. The fluorescence lifetime of the samples was recorded by the FLS-980 spectrometer.

2 Results and Discussion

2.1 Phase of products

Luminescence properties are always determined by the phase composition and the crystal structure of the host material. Fig. 1 shows the XRD patterns of $Y_2O_2SO_4$: Eu^{3+} samples sintered at different temperatures (950~1150 °C) for 2 h doped with 10mol% Eu^{3+}. All the diffraction peaks of the products match well with the standard monoclinic phase with a space group C2/c. The peaks with the strongest intensity correspond to the crystal planes (310). The molten salt method can reduce the preparation temperature of $Y_2O_2SO_4$: Eu^{3+} to 950 °C. The intensity of all peaks is gradually enhance as the temperature increases from 950 °C to 1100 °C, indicating the higher crystalline degree of the sample at a higher temperature. At 1150 °C, the diffraction peaks of the obtained product were indexed to the monoclinic Y_2O_3 phase, and the $Y_2O_2SO_4$ decomposed at high temperatures. Therefore, 1100 °C is chosen as a reasonable calcination temperature, which ensures the good crystallinity of the sample.

The monoclinic $Y_2O_2SO_4$ structure is built of alternative $Y_2O_2^{2+}$ layers and SO_4^{2-} layers; Y^{3+} and Eu^{3+} with a large ionic size occupy the distorted 8f sites with a coordination number of 8~9, and the edge-shared Y^{3+}/Eu^{3+}-$O^{2-}_{(8-9)}$ polyhedra form a chain along *c*-axis. The SO_4^{2-} tetrahedra with S^{6+} ions in the 4e sites are isolated between the $Y_2O_2^{2+}$ layers. The doping Eu^{3+} increases the lattice parameters of the structure. The amplified (310) reflection in Fig.2 demonstrates a slight shift toward the low-angle with increasing the concentration of doped Eu^{3+} because the ionic radius of Eu^{3+} (106.6 pm) is larger than that of Y^{3+} (101.9 pm). The lattice parameters of the samples increase with increasing the Eu^{3+} concentrations. As shown in Table 1.

2.2 Morphology of products

We used scanning electron microscopy to explore the microstructure and particle distribution of the $Y_2O_2SO_4$:Eu^{3+} (10 mol%). The morphological properties of $Y_2O_2SO_4$:Eu^{3+} sub-micron rods depend on the sintering temperatures (Fig. 3a~3f). Below 1000 °C, the morphology of the product is in the form of rice grain with a length of 3 μm, At 1050 °C, the length of micron rods increases, and there is some agglomeration between the particles. The $Y_2O_2SO_4$:Eu^{3+} rod fired at 1100 °C has

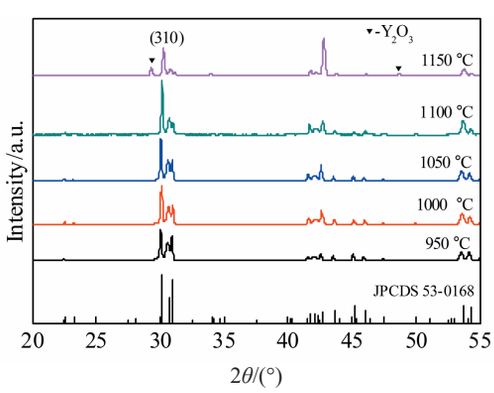

Fig.1 XRD patterns of $Y_2O_2SO_4$: Eu^{3+} samples sintered at different temperatures

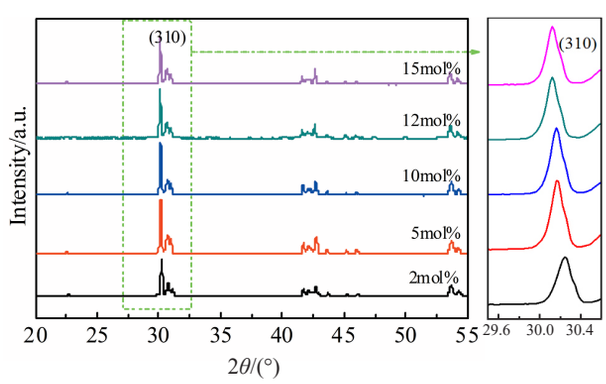

Fig.2 XRD patterns of $Y_2O_2SO_4$: Eu^{3+} samples with different Eu^{3+} concentrations

Table 1 XRD data and cell parameters of samples with different Eu^{3+} concentrations

Parameter	2mol%	5mol%	10mol%	12mol%	15mol%
(310) peak/(°)	30.24	30.16	30.15	30.14	30.11
a/nm	1.3278	1.3309	1.3315	1.3317	1.3318
b/nm	0.4133	0.4137	0.4140	0.4142	0.4149
c/nm	0.8009	0.8017	0.8019	0.8022	0.8024
$V/\times10^{-3}$ nm^3	421.66	421.99	422.57	422.76	422.90
$A=\gamma$/(°)	90	90	90	90	90
β/(°)	107.66	107.62	107.56	107.30	107.28

a larger length (> 10 μm) and a bigger length/width ratio than other samples; the sub-micron rods with a smooth surface and homogeneous particle size are straight and uniformly distributed. The particles split at 1150 °C, which is mainly caused by the decomposition of $Y_2O_2SO_4$. The molten salts form ionic liquids at relatively low temperatures and work as a chemical-reaction medium to create a liquid environment for crystal growth[25], providing the good dispersion, regular morphology and narrow particle size distribution of $Y_2O_2SO_4$:Eu^{3+} sub-micro rods prepared at 1100 °C. The element mapping of Y^{3+} and Eu^{3+} in Fig.3g and 3h shows uniform distribution in the sub-micron rods.

2.3 PL spectra of $Y_2O_2SO_4$:Eu^{3+}

Fig. 4 shows the excitation spectra of $Y_2O_2SO_4$: Eu^{3+} (10mol%) samples measured at the monitoring wavelength of 616 nm with a scanning range of 200~500 nm. All $Y_2O_2SO_4$: Eu^{3+} samples display similar PL spectra, and the change of sintering temperature has no effect on the shape and position of excitation spectra in $Y_2O_2SO_4$:Eu^{3+} system. The strong, broad band with a maximum peak at 270 nm is ascribed to the charge transfer state (CTS) of Eu^{3+} ions, which agrees well with the calculation result based on the equation: λ=1240/E[26,27]. Since the charge-transfer band is the result of the interaction of Eu^{3+} with coordination field and the strong coupling of lattice, the excitation spectrum has a wider spectrum. There are a series of narrow-band sharp excitation peaks in the long-band region, which are the electron absorption transition peaks of Eu^{3+}(f-f), and the excitation peaks at 395 and 460 nm correspond to the $^7F_0 \rightarrow {}^5L_6$ and $^7F_0 \rightarrow {}^5D_2$ transitions of Eu^{3+} ions, respectively. The excitation intensity is gradually enhanced as sintering temperature increases.

The room temperature emission spectra of $Y_2O_2SO_4$:Eu^{3+} (10mol%) excited by 270 nm UV light is shown in Fig.5. The emission spectrum of the sample consists of a group characteristic spectral lines of Eu^{3+}. The main emission peak located at 616 nm is the typical Eu^{3+} ion emission peak in rare earth oxysulfate host lattices, originating from the $^5D_0 \rightarrow {}^7F_2$ electric dipole transition of Eu^{3+} ions. The two emission peaks near 586 and 595 nm belong to the $^5D_0 \rightarrow {}^7F_1$ magnetic dipole transition of Eu^{3+} ions. Because the $^7F_1$ energy levels of the Eu^{3+} ions in the $Y_2O_2SO_4$ lattice split into two states at two non-identical locations, two asymmetric emission peaks from the two $^5D_0 \rightarrow {}^7F_1$ transitions are observed in the emission spectra[8]. Other characteristic emission peaks in Fig. 5 can be assigned to the $^5D_0 \rightarrow {}^7F_0$ (579 nm), $^5D_0 \rightarrow {}^7F_3$ (649 nm), and $^5D_0 \rightarrow {}^7F_4$ (699 and 704 nm) transitions of Eu^{3+} ions.

The intensity increases gradually from 950 to 1100 °C because of the better crystallization and fewer defects of the sample, which reduce the probabilities of light dispersion and non-radiative transition at high temperatures, as shown in Fig. 5. The luminescence intensity of the samples at 1150 °C begins to decrease, which is due to the decomposition of $Y_2O_2SO_4$.

The dopant concentration should influence the luminescent performance of the rare-earth ion activated materials, and when the Eu^{3+} doping concentration is low, the emitting center is insufficient, resulting in low luminescent intensity; however, concentration quenching will occur when Eu^{3+} concentration is beyond a critical value, so a series of $Y_2O_2SO_4$: Eu^{3+} phosphors with different compositions were synthesized to check the best doping concentration of Eu^{3+} ions in $Y_2O_2SO_4$. Fig.6 shows the emission spectra of $Y_2O_2SO_4$:Eu^{3+} with differ-

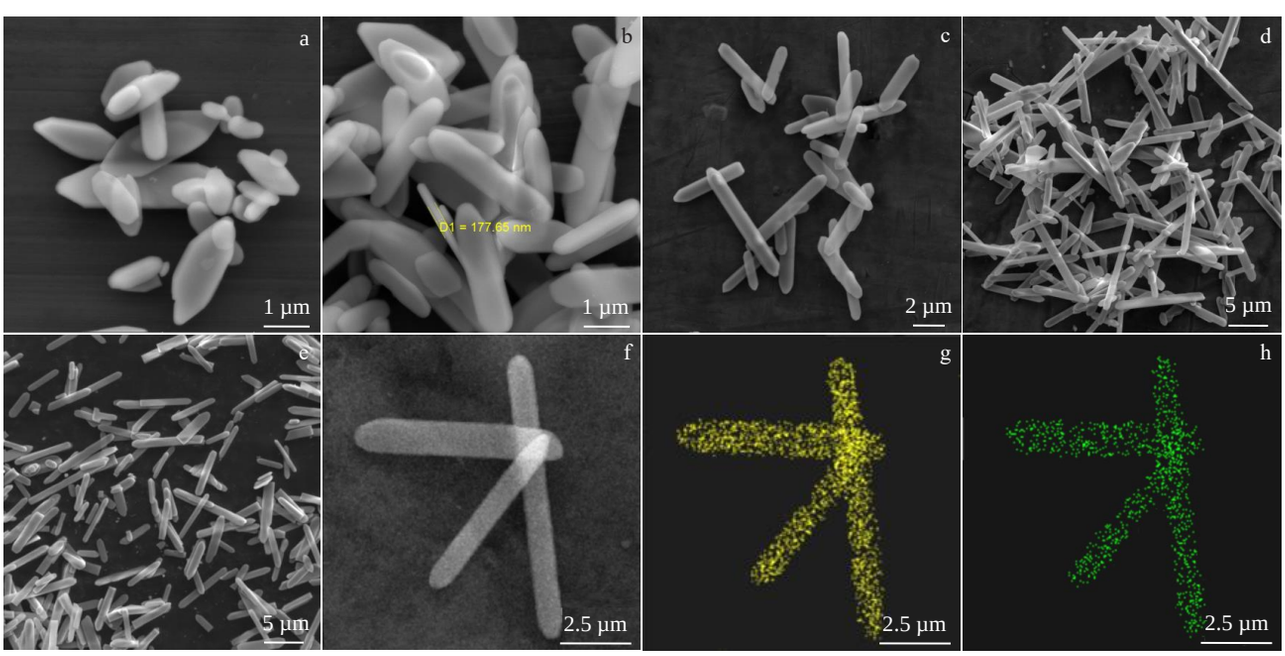

Fig.3 SEM images (a~e) of $Y_2O_2SO_4$:Eu^{3+} micron rods prepared at different temperatures: (a) 950 °C, (b) 1000 °C, (c) 1050 °C, (d) 1100 °C, (e) 1150 °C; EDS mapping of Y (g) and Eu (h) corresponding to SEM image of $Y_2O_2SO_4$:Eu^{3+} micron rods prepared at 1100 °C (f)

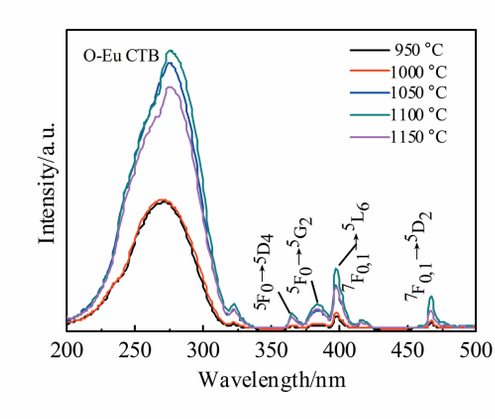

Fig.4 Excitation spectra of $Y_2O_2SO_4$: Eu^{3+} (10mol%) samples sintered at different temperatures

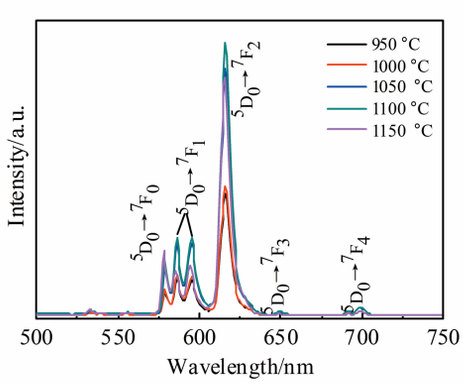

Fig.5 Emission spectra of $Y_2O_2SO_4$: Eu^{3+} (10mol%) samples sintered at different temperatures

ent Eu^{3+} concentrations, which were excited at 270 nm; all the samples were located at similar positions and the dopant content can greatly influence the emission intensity. As shown in Fig. 6, the emission intensity of $^5D_0\rightarrow{}^7F_2$ is enhanced as the Eu^{3+} concentration increases to 10mol%, but the concentration quenching effect, which is caused by the non-radiative energy transfer among luminous centers, takes place when the Eu^{3+} concentration is above 10mol%. The non-radiative energy transfer from an Eu^{3+} ion to another Eu^{3+} ion can be conducted through the following three ways: radiation reabsorption, exchange interaction, and electric multipole interaction. Radiation reabsorption requires an extensive overlap between emission and excitation spectra. However, from Fig. 4 and 5, the emission spectra and the excitation spectra almost do not overlap, indicating that radiative reabsorption can be neglected in this case. The exchange interaction requires a large overlap between the donor and the acceptor energy levels, which belongs to the forbidden transition and the smaller critical distance (< 0.5 nm). The critical distance (R_c) between Eu^{3+} ions in $Y_2O_2SO_4$:Eu^{3+} can be estimated by the following equation[28]:

$$R_c \approx 2\left(\frac{3V}{4X_cZ}\right)^{1/3} \quad (1)$$

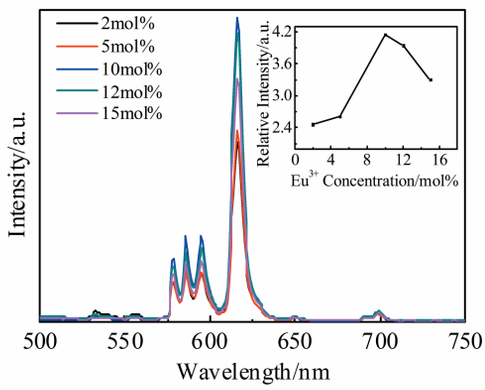

Fig.6 Emission spectra of $Y_2O_2SO_4$: Eu^{3+} with different concentrations of Eu^{3+} ions

where V is the volume of the unit cell, X_c is the critical concentration of Eu^{3+} ions, and Z is the number of cations in the unit cell. In the crystal cell structure of $Y_2O_2SO_4$:Eu^{3+}, the V and Z values are 422.6 and 8, respectively. Here, X_c is 0.1, and according to the above equation, the critical distance in the $Y_2O_2SO_4$:Eu^{3+} sub-micron rods is 1.46 nm, which is much larger than the limited critical distance (<0.5 nm). Therefore, the exchange interaction is not valid. Finally, the non-radiative energy transfer process of $Y_2O_2SO_4$: Eu^{3+} is possible due to the electric multipole interaction.

2.4 Color coordinate and fluorescence lifetime of the $Y_2O_2SO_4$:Eu^{3+}

Any color of light can be synthesized from red, green, and blue light. These three colors are usually referred to as the 1931 color coordinates. In general, the color of any light source in this color space can be represented as an (x, y) coordinate, and the color component of the light emitted by the phosphor can be obtained from the color coordinate diagram. The chromaticity properties of $Y_2O_2SO_4$: Eu^{3+} with different Eu^{3+} concentrations (Fig. 7) were studied. As the concentration of Eu^{3+} ions increases from 2mol% to 15mol%, the CIE chro-

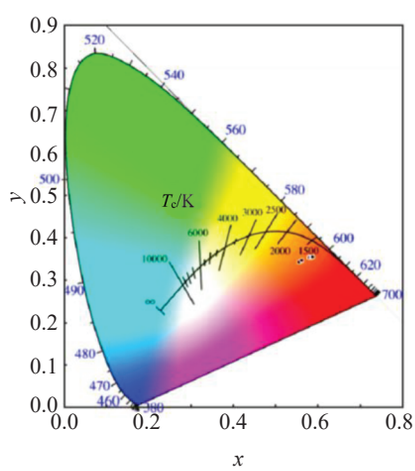

Fig.7 CIE chromaticity coordinate diagram of $Y_2O_2SO_4$: Eu^{3+} with different Eu^{3+} concentrations

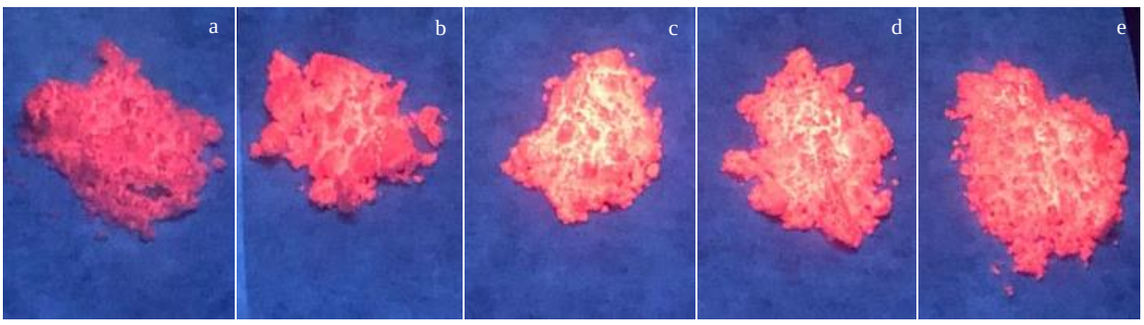

Fig.8 PL photos of $Y_2O_2SO_4:Eu^{3+}$ with different Eu^{3+} concentrations under 365 nm UV light excitation: (a) 2mol%, (b) 5mol%, (c) 10mol%, (d) 12mol%, and (e) 15mol%

maticity coordinates are calculated to be (0.5560, 0.3420), (0.5621, 0.3472), (0.5799, 0.3535), (0.5857, 0.3532), and (0.5886, 0.3541). However, the color coordinates of the samples gradually move from orange-red to red region. To further verify the change of the color, Fig.8 represents the PL photos of the sample with different Eu^{3+} concentrations under 365 nm UV light excitation. With the increase of Eu^{3+} concentration, the changes of luminescence intensity and color are consistent with the above PL emission spectra and CIE chromaticity diagram.

In order to further understand the nature of the PL dynamics, the fluorescence lifetime of $Y_2O_2SO_4:Eu^{3+}$ sub-micron rods with different doping concentrations was measured. Fig. 9 shows the decay curve of the $^5D_0 \rightarrow {}^7F_2$ transition for the $Y_2O_2SO_4:Eu^{3+}$ sub-micron rods excited at 275 nm and monitored at 616 nm. The PL intensity decays gradually to a steady-state value of about micro-seconds. The luminescence decay curves can be fitted into a single exponential function:

$$I = I_0 + A\exp(-t/\tau) \quad (2)$$

where I_0=17.62, A=5580.66, and τ is the corresponding time when the emission intensity of the $^5D_0 \rightarrow {}^7F_2$ transition of Eu^{3+} decays to 1/e of the initial intensity. According to the fitting results, the luminescent lifetime of the $Y_2O_2SO_4:Eu^{3+}$ sub-micron rods is 1.177, 1.173, 1.161, 1.156, and 1.153 ms, indicating that only one lattice site in the framework of $Y_2O_2SO_4:Eu^{3+}$ is occupied by the doped Eu^{3+} ions. The decay time decreases with increasing the doping concentration of Eu^{3+} from 2mol% to 15mol%.

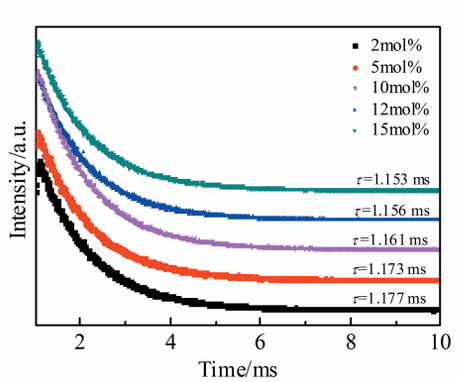

Fig.9 Decay curves of the $^5D_0 \rightarrow {}^7F_2$ transition for the $Y_2O_2SO_4:Eu^{3+}$ sub-micron rods with different Eu^{3+} concentrations (λ_{em}= 616 nm)

3 Conclusions

1) The monoclinic $Y_2O_2SO_4:Eu^{3+}$ (10mol%) sub-micron rods with a length more than 10 μm and a width of 500~800 nm can be successfully synthesized by a simple molten salt method.

2) The sub-micron rods sintered at 1100 °C has a narrow particle size distribution and a high degree of crystallization.

3) The strongest red emission peak at 616 nm of the $Y_2O_2SO_4:Eu^{3+}$ (10mol%) sample under the excitation of 270 nm ultraviolet light is originated from the $^5D_0 \rightarrow {}^7F_2$ transition of Eu^{3+}, and the transition emission exhibits a single exponential decay behavior with a lifetime of 1.161 ms.

4) Because of the large critical distance of the doped Eu^{3+} ions, the electric multipole interaction rather than the exchange interaction dominates the concentration quenching effect in the samples with a Eu^{3+} concentration above 10mol%.

References

1 Machado L, Azeredo M, Correa H *et al*. *Journal of Thermal Analysis and Calorimetry*[J], 2012, 107(1): 305

2 Tan Shuai, Li Dongmei. *Applied Catalysis A: General*[J], 2017, 544(25): 55

3 Sun Xinyuan, Jiang Daguo, Chen Shiwei *et al*. *Journal of the American Ceramic Society*[J], 2013, 96(5): 1483

4 Zhang Lin, Ma Fei, Guan Qingmei *et al*. *Journal of Alloys and Compounds*[J], 2019, 802(25): 173

5 Chen Fashen, Yang Cejun, Liu Xiaohe *et al*. *ACS Sustainable Chemistry Engineering*[J], 2018, 6(8): 10 463

6 Wang Xuejiao, Li Jiguang, Zhu Qi *et al*. *Journal of Alloys and Compounds*[J], 2014, 603(5): 28

7 Shoji M, Sakurai K. *Journal of Alloys and Compounds*[J],

2006, 426(1): 244
8 Kijima T, Shinbori T, Sekitab M. *Journal of Luminescence*[J], 2008, 128(3): 311
9 Srivastava A M, Setlur A A, Comanzo H A *et al*. *Optical Materials*[J], 2008, 30(10): 1499
10 Song Lixin, Du Pingfan, Jiang Qinxu *et al*. *Journal of Luminescence*[J], 2014, 150: 50
11 Xing T H, Song L X, Xiong J *et al*. *Advances in Applied Ceramics*[J], 2013, 112(8): 455
12 Chen Gen, Chen Fashen, Liu Xiaohe *et al*. *Nano Research*[J], 2014, 7: 1093
13 Lian Jingbao, Qin Hua, Liang Ping *et al*. *Solid State Sciences* [J], 2015, 48: 147
14 Wang Xudong, Li Zhaodong, Shi Jian *et al*. *Chemical Reviews* [J], 2014, 114(19): 9346
15 Xiao Fangxing, Miao Jianwei, Tao Huabing *et al*. *Small*[J], 2015, 11(18): 2115
16 Peng Yin, Yan Mei, Chen Qingguo *et al*. J*ournal of Materials Chemistry A*[J], 2014, 22: 8517
17 Reddy M V, Zhang Beichen, Loh K P *et al*. *Cryst Eng Comm* [J], 2013, 18: 3568
18 Reddy M V, Adams S, Galen Tiong Ji Liang *et al*. *Solid State Ionics*[J], 2014, 262: 120
19 Gan Lin, Mao Zhiyong, Xu Fangfang *et al*. *Ceramics International*[J], 2014, 40(3): 5067
20 Wang Yixian, Wang Yuwei, Liu Jialiang *et al*. *Carbon*[J], 2017, 122: 344
21 Hu Zhimi, Xiao Xu, Jin Huanyu *et al*. *Nature Communications* [J], 2017(8): 15 630
22 Deng Jiguang, He Shengnan, Xie Shaohua *et al*. *Environmental Science Technology*[J], 2015, 49(18): 11 089
23 Li Lihong, Deng Jinxia, Chen Jun *et al*. *Chemical Science*[J], 2016(7): 855
24 Zhou Ming, Ming Hong, Peng Jiaqing *et al*. *ECS Journal of Solid State Science and Technology*[J], 2017, 6(12): 175
25 Ekmekci M K, Erdem M, Mergen A *et al*. *Journal of Alloys and Compounds*[J], 2014, 591: 230
26 Dorenbos P. *Journal of Luminescence*[J], 2005, 111(1): 89
27 Li Xing, Lian Jingbao. *Optik*[J], 2016, 127(1): 401
28 Podhorodecki A, Banski M, Noculak A *et al*. *Nanoscale*[J], 2013, 5: 429

$Y_2O_2SO_4:Eu^{3+}$亚微米棒的合成及发光性能

王玉香[1,2]，钟盛文[1]，文小强[2]，张　骞[1]
(1. 江西理工大学 材料冶金化学学部，江西 赣州 341000)
(2. 赣州有色冶金研究所，江西 赣州 341000)

摘　要：以Na_2SO_4和K_2SO_4为熔盐，采用熔盐法合成了一维$Y_2O_2SO_4:Eu^{3+}$亚微米棒。应用X射线衍射、扫描电子显微镜和光谱仪等方法对合成产物的晶体结构、形貌和发光性能进行表征。考察了烧结温度、Eu^{3+}掺杂浓度对合成产物的晶体结构、形貌和发光性能的影响。结果表明，原料混合物在1100 ℃空气中煅烧2 h可合成纯相、表面光滑的$Y_2O_2SO_4:Eu^{3+}$亚微米棒，$Y_2O_2SO_4:Eu^{3+}$亚微米棒的长度大于10 μm，宽度为500~800 nm。在270 nm紫外光的激发下，$Y_2O_2SO_4:Eu^{3+}$亚微米棒呈红光发射，最强发射峰位于616 nm处，归属于Eu^{3+}的$^5D_0\rightarrow{}^7F_2$跃迁，$Y_2O_2SO_4:Eu^{3+}$亚微米棒Eu^{3+}的最佳掺杂浓度为10mol%。

关键词：熔盐法；$Y_2O_2SO_4$；Eu^{3+}亚微米棒；Eu^{3+}掺杂

作者简介：王玉香，女，1984年生，博士生，高级工程师，江西理工大学材料冶金化学学部，江西 赣州 341000，E-mail：wyx_522@126.com